

ITC 3/52 Information Technology and Control Vol. 52 / No. 3 / 2023 pp. 680-692 DOI 10.5755/j01.itc.52.3.33659	Deep Convolutional Generative Adversarial Networks for Automated Segmentation and Detection of Lung Adenocarcinoma Using Red Deer Optimization Algorithm	
	Received 2023/03/16	Accepted after revision 2023/05/31
	HOW TO CITE: Sasikumar, N., Senthilkumar, M. (2023). Deep Convolutional Generative Adversarial Networks for Automated Segmentation and Detection of Lung Adenocarcinoma Using Red Deer Optimization Algorithm. <i>Information Technology and Control</i> , 52(3), 680-692. https://doi.org/10.5755/j01.itc.52.3.33659	

Deep Convolutional Generative Adversarial Networks for Automated Segmentation and Detection of Lung Adenocarcinoma Using Red Deer Optimization Algorithm

N. Sasikumar

Department of Electronics and Communication Engineering, Paavai College of Engineering, Namakkal, 637018, India

M. Senthilkumar

Department of Electrical and Electronics Engineering, Sona College of Technology, Salem, 636003, India

Corresponding author: sasikumarres1@gmail.com

The diagnosis of early-stage lung cancer can be challenging due to several factors. Firstly, the asymptomatic nature of the disease means that it may not present any noticeable symptoms until it has progressed to later stages. Additionally, the use of computed tomography, which can be expensive and involves repetitive radiation exposure, can further complicate the diagnostic process. Even specialists may encounter difficulties when examining lung CT imagery to identify pulmonary nodules, particularly in the case of cell lung adenocarcinoma lesions. This paper suggests a unique deep learning-based Deep Convolutional Generative Adversarial Networks (DCGAN) model for lung cancer classification. The dataset utilized for the experimental purpose is accessed from the LUNA16 challenge database. This comprises 888 CT scans of the lungs. These images are initially segmented using Quick-CapsNet (QCN) model and applied with Red Deer Optimization (RDO) algorithm to extract the optimized features. Furthermore, the categorization between benign and malignant tumors is carried out using the DC-GAN model. The pulmonary nodule detection accuracy of the proposed model is 98.65%, indicating early-stage lung cancer. It is discovered to be superior to other existing techniques, such as sophisticated deep learning, straightforward machine learning, and hybrid methods applied to lung CT scans for nodule diagnosis. According to experimental findings, the suggested way can significantly help radiologists spot early lung cancer and facilitate prompt patient management.

KEYWORDS: Deep Convolutional GAN, Quick-CapsNet, Red deer Optimization, Lung adenocarcinoma.

1. Introduction

The number of lung cancer patients globally has increased, and the recurrence rate has gone up year after year due to the worsening of the environment brought on by more severe air pollution and variables like tobacco consumption and environmental toxins [33]. One of the malignancies with the most excellent fatality rates today is lung adenocarcinoma. Concern has grown over correctly identifying lung disease and stopping its occurrence and progression [18]. Most lung nodules are harmless, but some may be early signs of cancer. Lung nodules are abnormal growths within the lung that can either be either cancerous or benign [6]. According to recent studies, only 22% of lung cancer patients survive for at least five years. Early diagnosis can significantly increase lung cancer survival rate. Noncancerous and not propagating to other body areas are benign lesions [21]. By 2034, the World Health Organization (WHO) predicts that 25% of fatalities will be attributable to lung adenocarcinoma.

Computed Tomography, the most popular imaging method in healthcare, is frequently used to find lung malignancies. High-density precision in CT images allows for creating contrast pictures even for parts with minute density variations, such as mucous membranes in humans. Yet, the volume of medical imaging data is expanding quickly due to the ongoing advancement of imaging technology and the corresponding rise in clinical needs, particularly the introduction of elevated CT equipment. According to statistics [25], 92% of the information stored in hospitals is in the form of medical images, and as clinical technology progresses, this percentage is growing by 32% annually. At the same time, just 8% more qualified imaging specialist clinicians have been hired [13].

A whole lung CT scan session typically comprises around 125 to 275 pictures. Radiologists' diagnostic work has become progressively more difficult, demanding their psychological and physiological stamina [27]. It demonstrates how reading time for a single scan sequence increases while reading accuracy decreases. After looking directly at CT pictures for a while, human eyes will likely grow tired, resulting in muffled observations and erroneous interpretations. The research team at Johns Hopkins University in the United States conducted similar research. It concluded that there is a 30-40 percent chance that a

single imaging specialist will overlook the dark spot of clinically relevant lung nodules while diagnosing a chest CT [9]. Thus, doctors must use computers to aid in reading and diagnosis, enhancing the speed and precision of the latter.

Computer-aided diagnostic (CAD) technology has made significant strides recently due to the rapid growth of computer infrastructure and programming technologies. It has also gradually proven its therapeutic relevance in prognosis. Professional clinical diagnosis specialists use CAD software more frequently to aid in evaluation. The hospital's workflow eventually incorporates CAD software as a "serial device" [4]. Through the use of radiographic images, imagery analysis methods, and computerized analysis capabilities, physicians' assessment of individuals is enhanced to be more effective and precise.

Deep learning has tremendous potential for classifying cancerous and non-malignant cancer nodules since it may minimize the number of scans necessary to determine whether a nodule is benign or malignant [12]. Detecting harmless and cancerous modules using deep learning approaches has shown encouraging results. The most advanced CAD system uses deep learning models to characterize lung nodules and determine whether they are problematic [28]. These systems also identify a nodule's kind, determining whether it is harmful or innocuous.

Even though CAD systems show noticeably more excellent performance in lesion diagnosis, few studies take a regular physicians' workflow into account [23]. Clinically, physicians locate the suspicious prospects for additional evaluation by evaluating the Maximal Prediction Strength (MPS) images [30]. MPS enables higher spectral 3-D volumetric translation to the direction of extrapolation, improving tumor identification. Deep learning techniques can detect pulmonary nodules spontaneously since MPS images retain sensitivity data and are not boundary reliant [16]. Thus, this study proposes a deep learning-based approach incorporating segmentation and optimization techniques for lung cancer detection.

The main contributions of this work are,

- 1 To propose an innovative deep learning model such as Deep Convolutional Generative Adversar-

ial Networks to classify benign and malignant lung adenocarcinoma more precisely and reliably.

- 2 To efficiently segment the lung CT images using the Quick-CapsNet model and extract the most optimal features from the segmented images using the Red Deer Optimization algorithm.
- 3 To effectively demonstrate the suggested model's performance excellence against existing literature on lung cancer identification and categorization.

The remainder of this paper is organized as follows. Section 2 elaborates on the recent works in lung cancer research using deep learning approaches. Section 3 describes the proposed methodology to efficiently detect lung cancer from CT images using segmentation, optimization, and classification techniques. Section 4 presents the results of applying the proposed optimized deep learning model to the LUNA16 dataset. Section 5 discusses the challenges and research directions in this arena exclusively. Section 6 concludes the present research.

2. Related Works

This section discusses the various state-of-the-art methods in lung adenocarcinoma detection employing deep learning techniques. Authors in [5] introduced the three-dimensional convolutional neural networks-based unsupervised learning approach for lung cancer diagnosis. This statistical classification approach enhances pulmonary nodule transparency using the steepest descent non-linear activation [7]. The proposed detection technique is evaluated and contrasted with an existing two-dimensional convolutional neural network learning model using the LUNA dataset. As only 10% of the training database was used for testing, the suggested model is unsuccessful [31].

Researchers in [24] developed a supervised prediction algorithm to identify early adenocarcinoma in lung cancer patients. The suggested model was verified using real-time non-cancerous patient data collected from impacted individuals in the initial phases. The database contains 315 data phases that have been recorded [19]. The created model, a VGG network-based training classifier, has an unsatisfactory prediction rate of 74 percent Area under the curve. The VGG CNN model's flaw is that it needs to be pre-processed for CT semantic segmentation and image

filtering, which lowers the prediction rate [32].

The most recent methods for classifying and detecting lung cancer were evaluated in [8]. The most recent tumor segmentation identification, placement, and classifications are associated with algorithmic approaches to supervised learning like Support Vector Machine, K-nearest neighbors, and Convolutional neural networks and standard datasets like LIDC-ID-R1, LUNA 16 as well as Super Bowl Dataset 2016 considered to be the most common and typical baseline CT data for illness diagnosis [17]. To identify patients with aggressive or innocuous lung cancer, authors in [1, 14] presented the DenseNet model, a categorical predictor built on a dense CNN model. The researchers used a dataset of 204 lung scans [10], with 75% of the images used for training and 25% for validation and prediction. Test results showed that the suggested procedure had an accuracy of 91.65% [20].

After examining hyperspectral imagery, five different types of pulmonary and colorectal cells were identified using a grading system created by the scientists [2]. According to the results, the suggested model can successfully identify diseased tissue up to 93.33 percent of the time. According to [3], computer-assisted examinations can be used to collect, evaluate, and integrate multitype intertwined features to determine the status of a Missense mutation. This study uses a new hybrid network model based on the CNN model combined with Recurrent Neural Networks. Using CNN, image statistical features are collected, and connections between different feature set types are simulated.

Their results demonstrated that multitype reliance feature representations outperform single-type image features compared to the traditionally extracted characteristics. Researchers in [26] created a method using computer-aided diagnosis assistance systems for lung nodule diagnosis based on three-dimensional deep CNN to assist physicians. In this study, a computer-aided diagnosis (CAD) system was trained and validated using the LUNA16 and ANODE09 datasets. In [29, 15, 22], authors presented a novel customized deep learning technique that utilizes binary genetic algorithms with decision trees and convolutional neural networks to classify various types of cancer based on malignant RNA sequences of genomic information. Table 1 summarizes the existing methods for lung cancer diagnosis using deep learning techniques.

Table 1

Comparison of Existing approaches for Melanoma Diagnosis

Reference	Deep Learning technique	Dataset used	Inference	Accuracy obtained
[24]	Three-dimensional Deep CNN	LIDC-IDRI	The restrictions of the datasets used to train the models, such as the absence of significant nodule annotations, continue to constrain performance.	83%
[32]	Mask R-CNN	LUNA-16	There are certainly tiny, low-contrast nodules that go undetected.	85.5%
[8]	Optimal Deep Neural Network	LIDC-IDRI	Memory, as well as computational constraints, are high.	91%
[17]	Inception V3	LUNA-16	It can be utilized for early-stage cancer prediction	89.85%
[24]	DenseBTNet	LIDC-IDRI	It uses an optimized structure with relatively straightforward operations	93%
[11]	Deep Residual CNN	Cancer Imaging Archive (CIA)	Training time is low	90.75%

Thus, it is observed from the literature review that though deep learning is applied to detect lung cancer in various research, there still is a lot of scopes to perform the classification with more accuracy and resilience. Therefore, the proposed study also applies a deep learning model for classifying lung CT images using segmentation and optimization techniques.

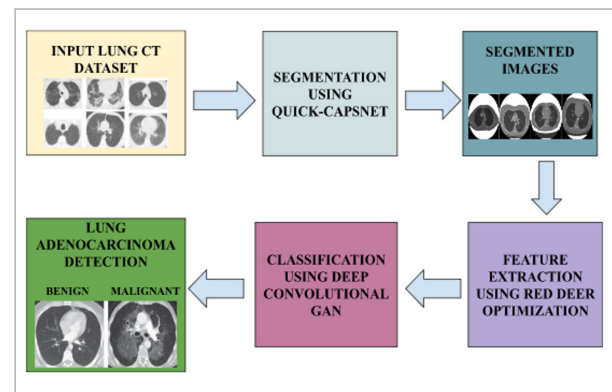
3. Proposed Methodology

This section discusses the proposed methodology for lung adenocarcinoma detection using Quick-CapsNet, Red deer Optimization algorithm, and Deep Convolutional GAN model. A detailed description of these models concerning the suggested approach is presented. The workflow of the proposed system is depicted in Figure 1.

Today medical arena depends on artificial intelligence for predicting the highly dangerous diseases in the human life. This research use deep learning and heuristic method to predict the lung adenocarcinoma detection. First, the dataset is collected and segmented using Quick-CapsNet algorithm. Segmented images are used for extracting the features using red deer optimization algorithm. Finally, extracted features

Figure 1

Proposed Architecture

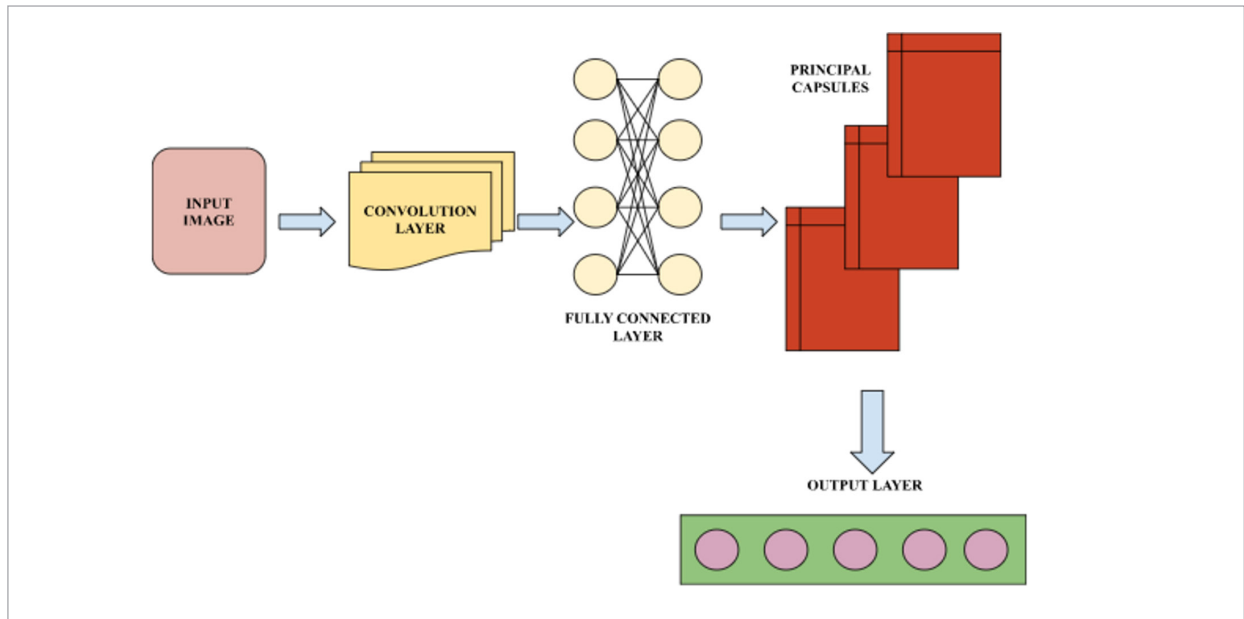


are tested with classification called as deep convolutional generative adversarial network. Figure 1 shows the architecture of proposed research work.

3.1. Quick-CapsNet (QCN)

In this work, QCN is employed to perform the segmentation process, an extension of the Capsule Networks. The architecture of QCN is elaborated on in this section. In conventional Capsule Networks, two convolutional layers that extract the input image's basic features are the network's first layers. 8D vectors are created by reshaping the second convolutional

Figure 2
QCN Architecture



layer's output. The term "Principal Capsules" refers to these 8D vectors. Once the initial layer of capsules is produced, there may be several further layers.

In the convolutional layer of Quick-CapsNet, the kernel size of 9 refers to the size of the filter or window that moves over the input image to perform convolution. Specifically, a 9x9 kernel is used to extract features from the input image, which are then used as input to subsequent layers in the network. The choice of kernel size can affect the performance of the network, as it determines the amount of spatial information that is captured from the input image. A larger kernel size can capture more global features, while a smaller kernel size can capture more local features.

In the QCN architecture shown in Figure 2, a Fully-Connected (FC) layer replaces the second convolution layer in the capsule network. This equates roughly to incorporating the participation of each neuron in the convolutional layer's output feature map. The FC layer describes all the neurons in the preceding layer. An FC layer is supplied with the output of the first convolutional layer. The Principal Capsules, which are the input for the route optimization algorithm, are constructed from the FC layer's output by reconfiguring it. The result of the segmentation is shown in Figure 3.

3.2. Red Deer Optimization Algorithm (RDOA)

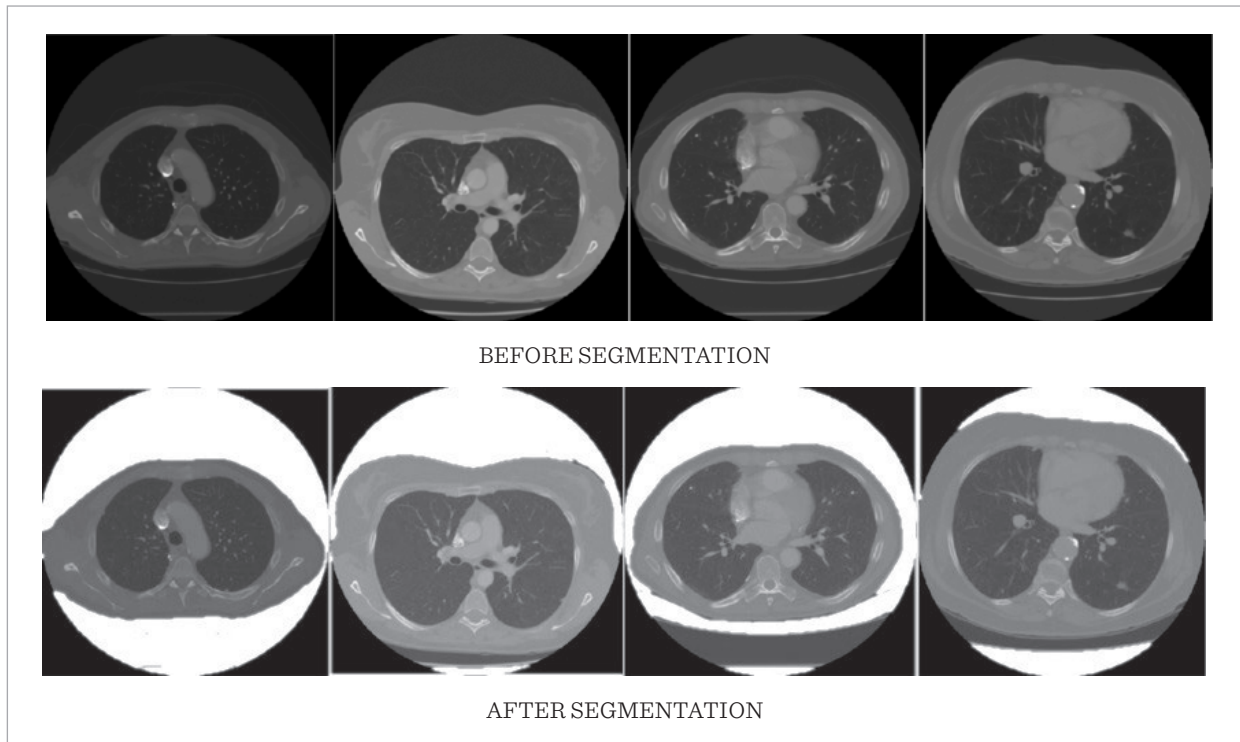
RDOA is used in the proposed work to select the optimized features before implementing the classification technique. The RDOA starts with a preliminary population of individuals opposite Red deers, just like other meta-heuristics. The population is divided into hinds and male red deers, with a chosen few of the top Red deers. The male red deer needs to roar first. They are split into two groups according to the intensity of a screaming phase, namely masters and stags. Then, each harem's masters and stags engage in joint combat to claim their respective harems. Moreover, masters create harems. The ability of the masters to scream and the battle is directly correlated with the number of hinds in harems. As a result, in harems, masters mate with various hinds. Figure 4 presents the steps in the Red deer Optimization Algorithm.

The initial population of individuals in the RDOA algorithm is defined as represented in (1),

$$RD_{pop} = [RD1, RD2, RD3, \dots, RDN]. \quad (1)$$

The above equation can be expressed as a value of the function as given in (2),

Figure 3
Segmentation Results



$$G(RD_{pop}) = G(RD1, RD2, RD3, \dots, RDN). \quad (2)$$

$$r_1, r_2, \text{ and } r_3$$

$$maleRD_{pos} = maleRD + r_1 \times ((U_{BD} - L_{BD}) * r_2) + L_{BD} \quad (3)$$

The above equation is applicable when the value of r_3 is greater than or equal to 0.5. For the vice-versa case, the equation is updated as shown in (4),

$$maleRD_{pos} = maleRD + r_1 \times ((U_{BD} - L_{BD}) * r_2) + L_{BD}. \quad (4)$$

The red deers are categorized into two groups namely the masters and the stags. The count of the masters among the male red deers is computed based on (5),

$$Total_{mastersRD} = \text{round} \{ \delta \cdot Total_{maleRD} \}, \quad (5)$$

where δ can be considered to be any value between 0 and 1.

The count of the stags in the male red deer group is determined using (6),

$$Total_{stageRD} = Total_{maleRD} - Total_{masterRD}. \quad (6)$$

With respect to the quarreling process between the masters and stags, it is possible to obtain two different solutions as denoted in (7) and (8) among which the optimal one is chosen.

$$maleRD_{sol1} = \frac{masterRD + stageRD}{2} + s_1 \times ((U_{BD} - L_{BD}) * s_2) + L_{BD} \quad (7)$$

$$maleRD_{sol1} = \frac{masterRD + stageRD}{2} - s_1 \times ((U_{BD} - L_{BD}) * s_2) + L_{BD}, \quad (8)$$

where s_1 and s_2 are the random values between zero and one.

The harems in the group are generated by splitting the hinds in the red deers group equally as in (9),

$$masterRD_{power} = masterRD_{norm} - \max \{ masterRD_k \} \quad (9)$$

$$mastersRD_{norm} = \left| \frac{mastersRD_{power}}{\sum_{k=1}^{Total} mastersRD_k} \right| \quad (10)$$

The count of the hinds for the corresponding harems is computed as shown in (11),

$$harem_{hind} = round \left\{ mastersRD_{norm} \cdot Total_{hind} \right\} \quad (11)$$

The coupling process between the masters and hinds is determined using equation (12),

$$maleRD_{sol3} = \frac{masterRD + harem_{hind}}{2} + \left((U_{BD} - L_{BD}) * d \right) \quad (12)$$

To calculate the count of the hinds available in the harems group which couples with the masters, (13) is utilized.

$$harem_{hind}^{couple} = round \left\{ \mu \cdot harem_{hind} \right\}. \quad (13)$$

In order to initiate the process of coupling between stag and hinds, it is essential to identify the distance between them. This is determined using (14),

$$dist_{stag}^{hind} = \left(\sum_{k=0}^N \left(stagRD_k - harem_{hind}^k \right)^2 \right)^{\frac{1}{2}}. \quad (14)$$

Algorithm 1. Red Deer Optimization Algorithm

Input: Initial population of individuals in red deers

Output: most optimal solution, RD^*

Step 1: Compute $maleRD$ and $Total_{hind}$

Step 2: Assign $RD' = optimalsolution$

Step 3: for each $maleRD$

Step 4: Compute location of $maleRD$ using (3) and (4)

Step 5: Modify location of $maleRD$ for optimal solutions

Step 6: end for

Step 7: Calculate $Total_{masterRD}$ and $Total_{stageRD}$ using (5) and (6)

Step 8: for each $masterRD$

Step 9: Create quarrel between $masterRD$ and $stageRD$ using (7) and (8)

Step 10: Modify the location of $masterRD$ and $stageRD$

Step 11: end for

Step 12: Create $harem_{hind}$ using (9), (10) and (11)

Step 13: for each $masterRD$

Step 14: Execute coupling process between $masterRD$ and $harem_{hind}$ using (12)

Step 15: Compute $harem_{hind}^{couple}$ using (13)

Step 16: end for

Step 17: for each $stageRD$

Step 18: Determine the distance between $stagsRD$ and $harem_{hind}$ using (14)

Step 19: Execute coupling process between $stageRD$ and $harem_{hind}$ using (12)

Step 20: end for

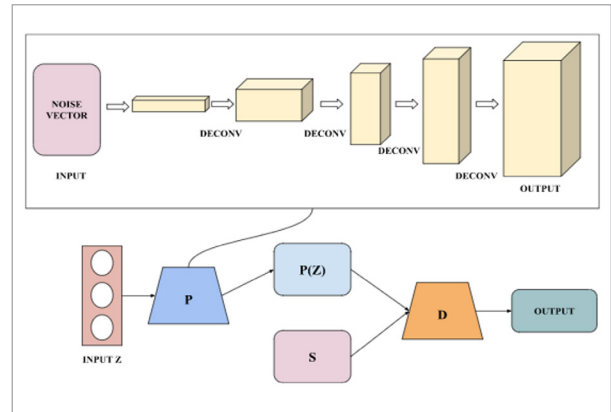
Step 21: Repeat the same for another generation of individuals and find most optimal RD^*

Step 22: return RD^*

Heuristics are problem-solving strategies that use rules of thumb, experience, and intuition to find solutions in complex situations. Heuristics can be applied in a variety of fields, from artificial intelligence to psychology, to help solve problems that are difficult to solve using traditional methods. Neuro-heuristics can be used to develop a system for pallet detection that uses neural networks to process sensory data and heuristic rules to guide the decision-making process.

Figure 4

DCGAN Architecture



3.3. Deep Convolutional GAN (DCGAN)

A Differentiator(D) and a Producer(P) are parts of GAN's primary structure. Real samples are generated using the producer, and real samples and fraudulent samples are distinguished by the differentiator. In order to produce a created false sample, the generator translates an additive noise field (Z) to a new multi-dimensional data structure. To perform classification and determine the likelihood that the testing sample (S) is a genuine sample, the differentiator is used. To create a false sample during training, the producer attempts to learn the data distribution of the real sample, while the differentiator aims to separate the resulting false sample from the real sample.

The deconvolution layer creatively replaced the fully connected layer of the producer in the basic GAN network, strengthening the neural network structure in the GAN model and attaining good performance in image creation tasks. As seen in Figure 4, the DCGAN uses CNN's strong feature extraction capabilities to enhance the generative network's capacity for learning. The layer's producer can learn steadily with the help of Regularization, allowing the model to understand better the distribution of the data sampled and more steadily provide elevated examples.

4. Results

In this section, the setup employed for conducting the experiments is briefly discussed, along with the details of the dataset used and metrics utilized to evaluate the performance of the proposed models. Further, the results obtained by applying the proposed model to the dataset are analyzed.

4.1. Experimental Setup

All experimental trials were executed with a singular Nvidia GeForce GTX 2080 Ti GPU. Deep learning models were developed using Keras and TensorFlow frameworks. Python was used as the programming language for code development purposes. Version 2.4.3 of Keras and 2.2.2 of TensorFlow were utilized in the proposed research.

4.2. Dataset Description

The divergent scans in the LUNA16 dataset, which is a subcategory of the LIDC-IDRI dataset, are screened

using several parameters. A substantial fraction should be used because pulmonary nodules might be minuscule. Scan results with a layer depth of more than 2.5 mm were thus disregarded. Moreover, images that had uneven layer separation or incomplete layers were dismissed. This resulted in 888 CT scans and 36,378 radiologists' observations. For lung cancer screening techniques, only the observations in this dataset labeled as nodules under 3 mm are considered significant [2]. Nodules discovered by various readers that were closer together than the product of their radii were combined. In this instance, the integrated annotations' locations and dimensions were normalized. As a result, a collection of 777, 2290, 1186, and 1602 nodules have, respectively, been evaluated by four radiologists. The dataset used in the experimentation can be accessed via the given link.

<https://www.kaggle.com/datasets/avc0706/luna16>

4.3. Performance Metrics

The various performance metrics such as Accuracy, Precision, Recall and F1 Score used to assess the performance of the proposed model are described below. Here represent the True positive, False Positive, True Negative and False Negative values respectively.

$$Accuracy = \frac{POS_T + NEC_T}{POS_T + POS_F + NEG_T + NEG_F} \quad (14)$$

$$Precision = \frac{POS_T}{POS_T + POS_F} \quad (15)$$

$$Recall = \frac{POS_T}{POS_T + NEG_F} \quad (16)$$

$$F1Score = 2 * \frac{Precision * Recall}{Precision + Recall} \quad (17)$$

4.4. Experimental Results

1000 initial samples were used in the proposed lung adenocarcinoma detection experiment. The data set was then extended using data augmentation to yield 10,000 samples, split into the training (80%) and the test set (20%). Two data augmentation techniques were applied to the dataset to enlarge it for trial purposes. First, the attempt to alter the axis of the images

was executed by flipping it. Secondly, image rotation was incorporated by generating an angle between 0 and 180 in an arbitrary fashion. The model parameters are set as per the details in Table 2.

Table 2

Model Parameter Settings

Model Parameters	Corresponding Values
Optimizer	Stochastic Gradient Descent Optimizer
Learning rate	0.1
Momentum	0.9
Weight decay	1e-4
Batch size	8
Epochs	100
Learning rate - Epoch 0 to 50	0.01
Learning rate - Epoch 51 to 70	0.001
Learning rate - Epoch 71 to 100	0.0001

Frame recognition is trained using the layer learning method since direct resizing of the image sequence would surely destroy a great deal of specific information and the problem of distorted boundaries. Frame retraining, the approach used, is comparable to the sliding window during feature extraction. The issue

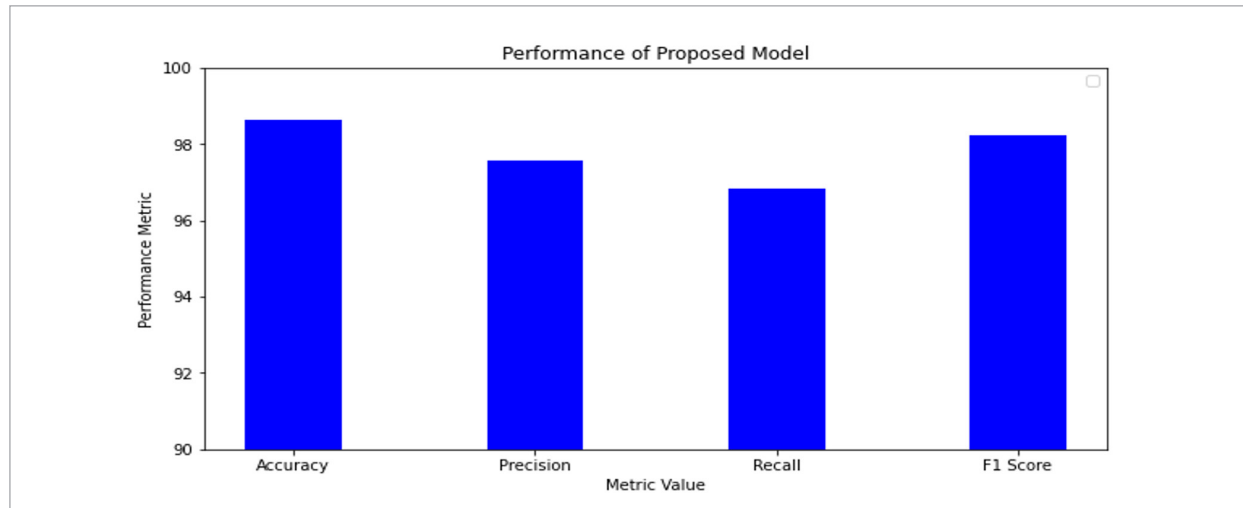
of surpassing the upper limit of the visual memory in the initial step of feature extraction can be avoided by partitioning the image information into 32 blocks, each of size 128. This increases the training data and prevents the input of the whole image.

The execution of the proposed model comprising the Deep Convolutional GAN with Red deer Optimization on the LUNA-16 dataset has achieved an accuracy of 98.65%. The precision, recall, and F1 score values are 97.56%, 96.85% and 98.25%. The obtained results are presented in graphical form in Figure 5. Further, the performance of the proposed model is compared with the conventional deep learning models and few of the existing works in the literature to prove the performance superiority of the suggested model for the diagnosis of lung adenocarcinoma

Deep learning models such as Deep Neural Networks (DNN), Convolutional Neural Networks (CNN), Recurrent Neural Networks (RNN), and Generative Adversarial Networks (GAN) are considered for the performance comparison with the proposed model initially. It is observed that DNN produced an accuracy of 83.56% for the lung cancer detection problem when applied to the LUNA-16 dataset. Precision, Recall, and F1 score values produced by this model are 82.45%, 81.75%, and 83.26%, respectively. The next model, CNN, made a better accuracy of 87.48% than DNN. The other performance metric values were also improved for the CNN model compared to the DNN

Figure 5

Performance of Proposed Model



model. Further, RNN produced an accuracy of 90.65%, a precision of 89.56%, a recall of 88.75%, and F1 score of 90.15%, correspondingly. The performance of the traditional GAN model for lung cancer classification is also analyzed to compare its performance against

the proposed model. GAN produced an accuracy level of 92.5% higher than the other Deep learning models applied to the lung cancer dataset. However, it is lower than the accuracy of cancer detection exhibited by the proposed DCGAN model, which is 98.65%.

Table 3

Conventional Deep learning models Vs Proposed model

Models	Accuracy (%)	Precision (%)	Recall (%)	F1 Score (%)
DNN	83.56	82.45	81.75	83.26
CNN	87.48	86.89	85.78	87.15
RNN	90.65	89.56	88.75	90.15
GAN	92.5	91.6	90.75	92.25
DCGAN	98.65	97.56	96.85	98.25

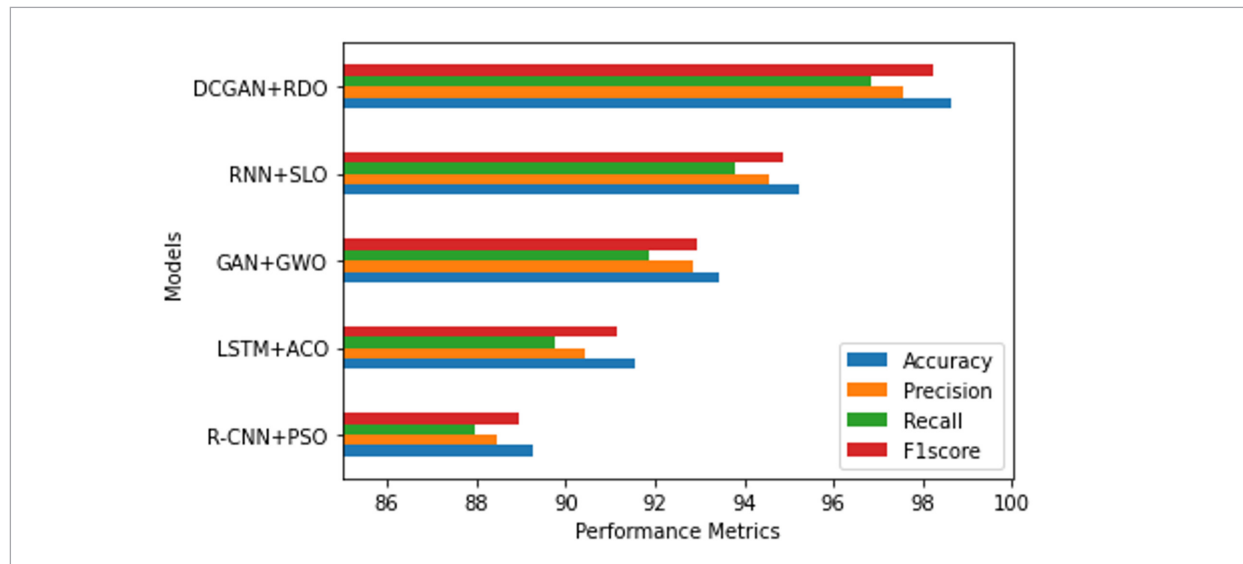
Table 4

Existing models Vs Proposed model

Models	Accuracy (%)	Precision (%)	Recall (%)	F1 Score (%)
R-CNN + PSO	89.25	88.45	87.98	88.95
LSTM + ACO	91.56	90.45	89.75	91.16
GAN + GWO	93.45	92.85	91.89	92.95
RNN + SLO	95.24	94.56	93.78	94.89
DCGAN+RDO	98.65	97.56	96.85	98.25

Figure 6

Performance Comparison Existing Vs Proposed



5. Discussion

Deep learning approaches such as Quick-CapsNet and DCGAN have shown successful segmentation as well as classification results respectively. Unfortunately, there are still a lot of issues with lung cancer detection using deep learning algorithms. Secondly, because there are not any established processes for acquiring medical images, clinicians have not completely embraced deep learning techniques for routine clinical practice. It might be reduced by combining the procurement processes. Second, deep learning approaches often need many well-labeled medical images to finish training objectives. Even when done by professional physicians, collecting a sizable labeled image dataset is expensive and time-consuming. The lack of labeled data can be overcome using a variety of techniques. For instance, transfer learning may address the training issue with limited samples. Computerized imagery fabrication, such as creating interaction networks, is another viable approach. Insufficient data will inevitably impact prediction accuracy and consistency. Consequently, one of the directions for future study is to increase the accuracy rate utilizing minimal supervision, transfer learning, and inter-learning with minimal labeled data.

6. Conclusion

In this research, a novel deep-learning model for lung adenocarcinoma detection and categorization

has been proposed. The proposed methodology primarily involved image segmentation, feature selection, and classification. The Quick-CapsNet model is incorporated to segment the images and feed them further for the feature selection process. Its ability to segment images quickly and accurately compared to other segmentation techniques. This is achieved by reducing the number of computations required for the segmentation process, making it computationally efficient. The red deer Optimization algorithm extracts optimized features from the segmented images before forwarding them to the classification phase. The segmented image can be represented as a matrix of pixels, where each pixel has a certain value that corresponds to its intensity or color. RDO can then be used to select the most relevant features from this matrix by optimizing an objective function. The third stage of lung cancer categorization is performed using the Deep Convolutional GAN model, which successfully classifies benign and malignant lesions with an accuracy of 98.65%. The proposed model performance is contrasted against several traditional deep learning models and existing optimization-classification model combinations in the literature to prove the performance precedence of the suggested work. One of the downsides of the present research is that it has been applied to a smaller dataset. In future research, artificial intelligence solutions can be leveraged for lung cancer prognosis to relatively larger datasets comprising CT images.

References

1. Abdulgani, A. F., Al Ahmad, M. Label-Free Normal and Cancer Cells Classification Combining Prony's Method and Optical Techniques. *IEEE Access*, 2020, 8, 32882-32890. <https://doi.org/10.1109/ACCESS.2020.2973468>
2. Ardila, D., Kiraly, A.P., Bharadwaj, S., Choi, B., Reicher, J.J., Peng, L., Tse, D., Ettemadi, M., Ye, W., Corrado, G. End-to-End Lung Cancer Screening with Three-Dimensional Deep Learning on Low-Dose Chest Computed Tomography. *Nature Medicine*, 2019, 25, 954-961. <https://doi.org/10.1038/s41591-019-0447-x>
3. Antonio, V.A.A., Ono, N., Saito, A., Sato, T., Altaf-Ul-Amin M, Kanaya S. Classification of Lung Adenocarcinoma Transcriptome Subtypes from Pathological Images Using Deep Convolutional Networks. *International Journal of Computer Assisted Radiology and Surgery*, 2018, 1905-1913. <https://doi.org/10.1007/s11548-018-1835-2>
4. Bade, B.C., Dela Cruz, C.S., Lung Cancer 2020: Epidemiology, Etiology, and Prevention. *Clinics in Chest Medicine*, 2020, 41(1), 1-24. <https://doi.org/10.1016/j.ccm.2019.10.001>
5. Bicakci, M., Zaferaydin, O., Seyhankaracavus, A., Yilmaz, B. Metabolic Imaging Based Sub-Classification of Lung Cancer. *IEEE Access*, 2020, 8, 218470-218476. <https://doi.org/10.1109/ACCESS.2020.3040155>
6. Cerfolio, R. J., Moore, W. H. Can CT Radiomics Differentiate Benign from Malignant N2 Adenopathy in Non-Small Cell Lung Cancer. *Translational Lung Cancer Research*, 2020, 9(5), 1710-1711. <https://doi.org/10.21037/tlcr-20-477>

7. Chaturvedi, P., Jham, A., Vanani, M., Nemat, V. Prediction and Classification of Lung Cancer Using Machine Learning Techniques. *Materials Science and Engineering*, 2021, 1099(1), 012059. <https://doi.org/10.1088/1757-899X/1099/1/012059>
8. Chaunzw, T. L., Hosny, A., Xu, Y. Deep Learning Classification of Lung Cancer Histology Using CT Images. *Scientific Reports*, 2021, 11. <https://doi.org/10.1038/s41598-021-84630-x>
9. Farsad, M. FDG PET/CT in the Staging of Lung Cancer. *Current Radiopharmaceuticals*, 2020, 13(3), 195-203. <https://doi.org/10.2174/1874471013666191223153755>
10. Gopi, K., Selvakumar, J. Analysis of Lung Tumour Detection and Segmentation Using Level Set Method of Active Contour Model. *International Journal of Engineering & Technology*, 2018, 7(4), 410-441. <https://doi.org/10.14419/ijet.v7i4.10.21028>
11. He, Q., Qiu, Z., Tong, Y., Song, K. A New TTZ Feature Extracting Algorithm to Decipher Tobacco Related Mutation Signature Genes for the Personalized Lung Adenocarcinoma Treatment. *IEEE Access*, 2020, 8, 89031-89040. <https://doi.org/10.1109/ACCESS.2020.2993118>
12. Hu, M., Zhong, S. Xie, Lv, H., Lv, Z. Fuzzy System-based Medical Image Processing for Brain Disease Prediction, *Frontiers in Neuroscience*, 2021, 15(15), 714318. <https://doi.org/10.3389/fnins.2021.714318>
13. Hu, W., Liu, Z., Xiao, X., Yang, Y., Sun, Z., Wang, X. Comparison of Diagnostic Efficacy of MRI and PET/CT in Lung Cancer of Mouse with Spinal Metastasis. *Cellular and Molecular Biology (Noisy-le-Grand, France)*, 2020, 66(3), 138-142. <https://doi.org/10.14715/cmb/2020.66.3.21>
14. Jagadeesh Kumar, S. J. K., Parthasarathi, P., Hogo, Mofreh A., Masud, Mehedi, Al-Amri, Jehad F., Abouhawwash, Mohamed. Breast Cancer Detection Using Breastnet-18 Augmentation with Fine Tuned Vgg-16s. *Intelligent Automation & Soft Computing*, 2023, 36(2), 2363-2378. <https://doi.org/10.32604/iasc.2023.033800>
15. Jaszcz, A., Połap, D., Damaševičius, R. Lung X-ray Image Segmentation Using Heuristic Red Fox Optimization Algorithm. *Scientific Programming*, 2022, 1-8. <https://doi.org/10.1155/2022/4494139>
16. Jonas, D. E., Reuland, D. S., Reddy, S. M. Screening for Lung Cancer with Low-Dose Computed Tomography. *Journal of the American Medical Association*, 2021, 325(10), 971-987. <https://doi.org/10.1001/jama.2021.0377>
17. Kalaivani, N., Manimaran, N., Sophia, S., Devi, D.D. Deep Learning based Lung Cancer Detection and Classification. *IOP Conference Series: Materials Science and Engineering*, 2020, 994(1), 012026. <https://doi.org/10.1088/1757-899X/994/1/012026>
18. Li, Y., Zhao, J., Lv, Z., Li, J. Medical Image Fusion Method by Deep Learning. *International Journal of Cognitive Computing in Engineering*, 2021, 2, 21-29. <https://doi.org/10.1016/j.ijcce.2020.12.004>
19. Liu, Z., Zhang, G., Jingyuan, Z. Second-Generation Sequencing with Deep Reinforcement Learning for Lung Infection Detection. *Journal of Healthcare Engineering*, 2020, 2020, 3264801. <https://doi.org/10.1155/2020/3264801>
20. Masood, A., Sheng, B., Li, P. Computer-Assisted Decision Support System in Pulmonary Cancer Detection and Stage Classification on CT Images. *Journal of Biomedical Informatics*, 2018, 79, 117-128. <https://doi.org/10.1016/j.jbi.2018.01.005>
21. National Lung Screening Trial Research Team, Lung Cancer Incidence and Mortality with Extended Follow-Up in then National Lung Screening Trial. *Journal of Thoracic Oncology*, 2019, 14(10), 1732-1742. <https://doi.org/10.1016/j.jtho.2019.05.044>
22. Połap, D., Woźniak, M., Damaševičius, R., Wei, W. Chest Radiographs Segmentation by the Use of Nature-Inspired Algorithm for Lung Disease Detection. *Proceedings of the 2018 IEEE Symposium Series on Computational Intelligence, SSCI 2018*, 2019, 2298-2303. <https://doi.org/10.1109/SSCI.2018.8628869>
23. Savic, M., Ma, Y., Ramponi, G., Du, W., Peng, Y. Lung Nodule Segmentation with a Region-based Fast Marching Method. *Sensors*, 2021, 21(5), 1908. <https://doi.org/10.3390/s21051908>
24. Serj, M.F., Lavi, B., Hoff, G. A Deep Convolutional Neural Network for Lung Cancer Diagnostic. *Computer Vision and Pattern Recognition*, 2018, 1.
25. Shan, Y., Yin, X., Zhao, N., Wang, J., Yang, S. Comparison of Serum Tumor Markers Combined with Dual-Source CT in the Diagnosis of Lung Cancer. *Minerva Medica*, 2021, 19. <https://doi.org/10.23736/S0026-4806.21.07124-X>
26. Shiwen, S., Simon, X.H., Denise, R.A., ATB, A., William, H. An Interpretable Deep Hierarchical Semantic Convolutional Neural Network for Lung Nodule Malignancy Classification. *Expert Systems with Applications*, 2019.

27. Spiro, J. E., Rinneburger, M., Hedderich, D. M. Monitoring Treatment Effects in Lung Cancer-Bearing Mice: Clinical CT and Clinical MRI Compared to Micro-CT. *European Radiology Experimental*, 2020, 4(1), 31. <https://doi.org/10.1186/s41747-020-00160-7>
28. Thakur, S. K., Singh, D. P., Choudhary, J. Lung Cancer Identification: A Review on Detection and Classification. *Cancer Metastasis Reviews*, 2020, 39(3), 989-998. <https://doi.org/10.1007/s10555-020-09901-x>
29. Wang, C., Tyagi, N., Rimner, A., Hu, Y. C., Veeraraghavan, H., Li, G., Hunt, M., Mageras, G., Zhang, P. Segmenting Lung Tumors on Longitudinal Imaging Studies via a Patient-Specific Adaptive Convolutional Neural Network. *Radiother Oncol*, 2019, 101-107. <https://doi.org/10.1016/j.radonc.2018.10.037>
30. Xiao, Z., Liu, B., Geng, L., Zhang, F., Liu, Y. Segmentation of Lung Nodules Using Improved 3D-UNet Neural Network. *Symmetry*, 2020, 12(11), 1787. <https://doi.org/10.3390/sym12111787>
31. Valluru, D., Jeya, I.J.S. IoT with Cloud based Lung Cancer Diagnosis Model using Optimal Support Vector Machine. *Health Care Management Science*, 2020, 23(4), 670-679. <https://doi.org/10.1007/s10729-019-09489-x>
32. Zhang, R., Cheng, C., Zhao, X., Li, X. Multiscale Mask R-CNN-based Lung Tumor Detection Using PET Imaging. *Molecular imaging*, 2019, 18, 153601211986353. <https://doi.org/10.1177/1536012119863531>
33. Zhang, C., Li, J., Huang, J., Wu, S. Computed Tomography Image under Convolutional Neural Network Deep Learning Algorithm in Pulmonary Nodule Detection and Lung Function Examination. *Journal of Healthcare Engineering*, 2021, 2021(2021), 1-9. <https://doi.org/10.1155/2021/3417285>

